Second-order Dirac superconductors and magnetic field induced Majorana hinge modes

Sayed Ali Akbar Ghorashi[1], Xiang Hu[1], Taylor L. Hughes[2], Enrico Rossi[1]
[1]*Department of Physics, William & Mary, Williamsburg, Virginia 23187, USA and*
[2]*Department of Physics and Institute for Condensed Matter Theory, University of Illinois at Urbana-Champaign, IL 61801, USA*

(Dated: January 24, 2019)

We identify three dimensional higher-order superconductors characterized by the coexistence of one-dimensional Majorana hinge states and gapped or gapless surface sates. We show how such superconductors can be obtained starting from the model of a spinful quadrupolar semimetal with two orbitals and adding an s-wave superconducting pairing term. By considering all the possible s-wave pairings satisfying Fermi-Dirac statistics we obtain six different superconducting models. We find that for two of these models a flat-band of hinge Majorana states coexist with surface states, and that these models have a non-vanishing quadrupole-like topological invariant. Two of the other models exhibit hinge states in the presence of superconductivity and an additional Zeeman term in which case the hinge states are helical, dispersive, and localized only at two of the four hinges. We find that these states are protected by combinations of rotation and mirror symmetries, and the pair of corners exhibiting hinges states switches upon a change of sign of the Zeeman term. Furthermore, these states can be reduced to a single hinge with suitable perturbations. The remaining two models retain gapless bulk and surface states that spectroscopically obscure any possible hinge states.

The modern theory of polarization for crystalline insulators [1] has revealed that in crystals a dipole moment can be expressed in terms of Berry phases, and that a finite dipole necessarily implies the presence of boundary charges. The presence of nontrivial Berry phases and boundary states are the hallmarks of topological systems [2], and indeed it is now clear that there is a strong connection between the theory of topological insulators (TIs) and systems with quantized dipole moments[3–5]. This connection has led to the realization that the extension of the modern theory of polarization to higher multipole moments allows the identification of new classes of topological crystalline insulators [6, 7], termed "higher-order" TIs. Within this framework, a higher-order multipole TI of order m has a quantized nonzero electric m^{th}-pole in the bulk (with $m = 1$ for a dipole, $m = 2$ for a quadrupole,...) and localized charges at its $d - m$-dimensional boundaries, d being the insulator's spatial dimension. Since the work of Refs. 6 and 7 many proposals of higher-order TIs of various types have been presented [8–12]. Higher-order topological insulating phases have been realized in metamaterial arrays [13–15], and it has been proposed that bismuth [10], strained SnTe[8], and some 2D transition metal dichalcogenides [16] are second-order TIs. In addition, there has been exciting new work on higher order topological superconductors and topological semimetals [9, 16–23].

In this work we study superconducting instabilities of a 3D higher order topological quadrupolar semimetal. We focus on superconducting states obtained through s-wave superconducting pairing, and identify 3D higher-order topological superconductors that may manifest surface and/or hinge states, as summarized in Fig. 1. We find that some of the higher-order topological superconductors that we obtain are gapped in the bulk, but have 2D nodal Dirac superconductors on their surfaces, and flat bands of quasiparticle states on their hinges. We term such superconductors *second-order Dirac superconductors* Fig. 1 (a). We also obtain higher-order topological superconductors with gapped surfaces and non-chiral hinge states protected by a combination of C_4 and mirror symmetry. The hinge states are only present when the surfaces are gapped by a Zeeman term (Fig. 1 (b)), and are localized at only two of the four hinges (see Refs. 22 and 24 for insulating examples of states localized on two corners). Furthermore, the pair of corners (which are related by C_2 symmetry) that exhibit the 1D non-chiral states is controlled by the sign of the Zeeman term.

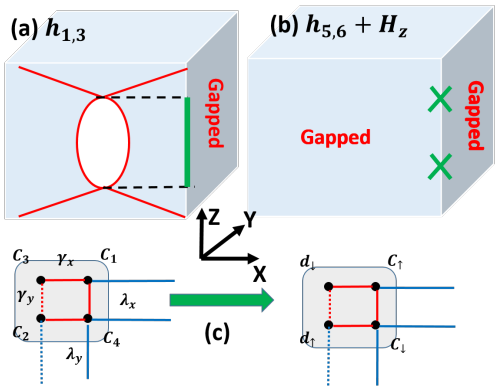

FIG. 1. Summary illustration of the models with hinge modes studied in this work. (a) model h_1 (rotate by C_4 for model h_3). (b) models $h_{5,6}$ with magnetic field (Zeeman term H_z) in the z-direction. Red lines represent surface states for $k_{x,y} = 0$ cuts. Green lines represent flat-band hinge states; green crosses represent dispersing hinge nodes. (c) The unit cell convention used to convert between spinless and spinfull version of HOTI and HOTSM.

We start by considering a model for a topological quadrupolar semimetal constructed from layers of 2D quadrupolar topological insulators [25]. Schematically, the unit cell for the tight binding model for the 2D quadrupolar insulator layer is illustrated in Fig. 1 (c). For each cell we have two orbitals (c, d) and a spin-1/2 degree of freedom, represented by the four black dots in Fig. 1 (c). Let γ_i ($i = x, y$) be the intra-cell hopping amplitudes, red lines in Fig. 1 (c), and λ_i

the inter-cell hopping, blue lines in Fig. 1 (c). Hopping processes represented by dotted lines have a phase that is opposite to the one of the hopping processes represented by solid lines. Depending on the choice of interlayer tunneling terms between quadrupole layers we obtain different Hamiltonians, H, for the resulting 3D system. In a momentum space basis we have $H_{\rm SM} = \sum_{\mathbf{k}} \psi^\dagger_{\mathbf{k}} h_{\rm SM}(\mathbf{k}) \psi_{\mathbf{k}}$, where $\psi^T_{\mathbf{k}}$ is the spinor $(c_{\mathbf{k}\uparrow}, d_{\mathbf{k}\uparrow}, d_{\mathbf{k}\downarrow}, c_{\mathbf{k}\downarrow})$, formed by the annihilation operators $c_{\mathbf{k}\alpha}$, $d_{\mathbf{k}\alpha}$, for an electron in orbital c, d, with spin α and momentum $\mathbf{k}$, and $h_{\rm SM}$ is a 4×4 Bloch Hamiltonian matrix of the general form:

$$h_{\rm SM}(\mathbf{k}) = (\gamma_x + \chi_x(k_z) + \lambda_x \cos(k_x))\Gamma_4 + \lambda_x \sin(k_x)\Gamma_3 + (\gamma_y + \chi_y(k_z) + \lambda_y \cos(k_y))\Gamma_2 + \lambda_y \sin(k_y)\Gamma_1. \quad (1)$$

In Eq. (1) all the lattice constants are taken to be 1, $\chi_i(k_z)$ $(i = x, y)$ are periodic functions of k_z with forms fixed by the interlayer tunneling terms, $\{\Gamma_\alpha\}$ are the 4×4 matrices given by the direct product of 2×2 Pauli matrices σ_i, κ_i in spin and orbital space, respectively: $\Gamma_0 = \sigma_3\kappa_0$, $\Gamma_i = -\sigma_2\kappa_i$, $\Gamma_4 = \sigma_1\kappa_0$. In the remainder we assume $\chi_i(k_z)$, γ_i, λ_i to be independent of the in-plane direction (x or y) such that the normal state topological quadrupolar semimetal has C_4 symmetry. To be explicit we will set $\lambda_i = \lambda$ and use it as our unit of energy with $\lambda = 1$. We then set $\chi_i(k_z) = \cos(k_z)/2$, and $\gamma_i = \gamma = -3/4$. With this choice of parametrization, $h_{\rm SM}(\mathbf{k})$ has fixed k_z "momentum slices" with a non-vanishing quantized quadrupole moment for $\cos(k_z) < -1/2$, and vanishing quadrupole for $\cos(k_z) > -1/2$. As a consequence, the bulk bands are semimetallic with four-fold degenerate nodes at the locations $k_z^{(c)}$ where the quadrupole changes, i.e., $\cos(k_z^{(c)}) = -1/2$ [25].

Model	Λ_i	$\mathcal{M}_x$	$\mathcal{M}_y$	$\mathcal{C}_4$	Structure	HOTSC
$h_{\rm SC,1}$	$\sigma_1\kappa_2$	$\tau_3 m_x$	$\tau_3 m_y$	-	intra-S	✓
$h_{\rm SC,2}$	$\sigma_2\kappa_1$	$\tau_0 m_x$	$\tau_3 m_y$	-	intra-S	✓
$h_{\rm SC,3}$	$\sigma_2\kappa_0$	$\tau_3 m_x$	$\tau_3 m_y$	-	inter-S	✓
$h_{\rm SC,4}$	$\sigma_2\kappa_3$	$\tau_3 m_x$	$\tau_0 m_y$	-	inter-T	✓
$h_{\rm SC,5}$	$\sigma_0\kappa_2$	$\tau_3 m_x$	$\tau_3 m_y$	$\tau_0\hat{r}_4$	inter-S	–(✓*)
$h_{\rm SC,6}$	$\sigma_3\kappa_2$	$\tau_0 m_x$	$\tau_0 m_y$	$\tau_3\hat{r}_4$	intra-T	–(✓*)

TABLE I. The pairings for the six different models discussed in this work. Columns 2-4 show the representation of the pairing term and of the symmetry operators for each model. $m_x = \sigma_1\kappa_3$, $m_y = \sigma_1\kappa_1$, $\hat{r}_4 = \frac{i}{2}(\sigma_1 + i\sigma_2)\kappa_2 + \frac{1}{2}(\sigma_1 - i\sigma_2)\kappa_0$. Column 6 shows the pairing structure: inter/intra and S/T are short for inter/intra orbital and spin singlet/triplet, respectively. Column 7 shows whether the model is a HOTSC: models with "*" in the parenthesis denotes existence of HOTSC in the presence of magnetic field.

The most general mean-field Hamiltonian describing a superconducting state for our system is given by $H_{\rm SC} = \sum_{\mathbf{k}} \Psi^\dagger_{\mathbf{k}} h_{\rm SC}(\mathbf{k}) \Psi_{\mathbf{k}}$ where $\Psi^T_{\mathbf{k}} = (\psi_{\mathbf{k}}, \psi^\dagger_{-\mathbf{k}})$ is the spinor in Nambu space and $h_{\rm SC}(\mathbf{k}) = \tau_3(h_{SM}(\mathbf{k}) - \mu) + \Delta_0^{(ij)}(\mathbf{k})\tau_2\sigma_i\kappa_j$, where μ is the chemical potential, $\Delta_0^{(ij)}(\mathbf{k})$ the superconducting pairing strength in the (ij) spin orbital channel, and $\{\tau_i\}$ are the Pauli matrices in Nambu space. Restricting the superconducting pairing to be s-wave, i.e., $\Delta_0^{(ij)}(\mathbf{k}) = \text{const} = \Delta_0$, we obtain

$$h_{\rm SC,i} = \tau_3(h_{\rm SM}(\mathbf{k}) - \mu) - \Delta_0\tau_2\Lambda_i \quad (2)$$

where Λ_i is a 4×4 matrix, independent of $\mathbf{k}$, that determines the structure of the superconducting pairing in orbital and spin space. The requirement that the pairing term satisfies Fermi-Dirac statistics implies that there are only six possible pairing matrices Λ_i, listed in the second column of Table I, (see e.g., [26]). As a consequence, starting from $h_{\rm SM}$, we can obtain six distinct s-wave superconducting states.

The normal state already has broken time-reversal symmetry ($T^2 = -1$), when the superconducting pairing is added these superconductors belong to symmetry class D [2]. We note that, as written, our model has a fine-tuned chiral symmetry but its presence is not required for our results. All the models have mirror symmetries in $\mathcal{M}_x$, $\mathcal{M}_y$, and $\mathcal{M}_z$, and therefore overall inversion symmetry $\mathcal{I} = \mathcal{M}_x\mathcal{M}_y\mathcal{M}_z$. The representation matrices for the $\mathcal{M}_x$ and $\mathcal{M}_y$ mirror symmetries are shown in Table I, and the matrix for $\mathcal{M}_z$ is the identity matrix. Models $h_{\rm SC,5}$ $h_{\rm SC,6}$, retain C_4 symmetry in the superconducting state with representation matrices given in Table I.

We can analyze the bulk quasi-particle spectra by considering the effects of Δ_0 perturbatively on the normal state semimetal by using a continuum $\mathbf{k}\cdot\mathbf{p}$ expansion around the nodes at the two $k_z^{(c)}$. The 16×16 continuum Hamiltonian is

$$H_{\mathbf{k}\cdot\mathbf{p},i} = -\tau_3\pi_0\sigma_2(vk_x\kappa_3 + vk_y\kappa_1) + v_z k_z(\tau_3\pi_3\sigma_2\kappa_2 - \tau_3\pi_3\sigma_1\kappa_0) - \mu\tau_3\pi_0\sigma_0\kappa_0 - \Delta_0\tau_2\pi_1\Lambda_i \quad (3)$$

where π_i are Pauli matrices in the valley/node degree of freedom, and v, v_z are velocities ($\hbar = 1$). In the nodal limit $\mu \to 0$, one can determine the nature of the bulk spectra by calculating how the pairing term commutes/anti-commutes with the kinetic terms. However, we are interested in the weak pairing limit, $\Delta_0 < \mu$. To understand this limit, we choose $\mu = 1, \Delta_0 = 0.5$. For this choice we find that models $h_{SC,1}, h_{SC,3}, h_{SC,6}$ are fully gapped in the bulk by the pairing term while $h_{SC,2}, h_{SC,4}, h_{SC,5}$ are gapless. Model $h_{SC,2}$ ($h_{SC,4}$) has gapless, bulk quasi-particle states forming a nodal line/loop in $k_x - k_z$ ($k_y - k_z$) plane, and model h_5 has 4 nodes in the $k_x - k_y$ plane at k_z values away from any high-symmetry points. We see that models $h_{\rm SC,1}$ and $h_{\rm SC,3}$ have the same symmetry, the same representation for $\mathcal{M}_x$ and $\mathcal{M}_y$, and have the same bulk spectra. Thus, they will have the same essential properties for our study, and henceforth we only consider $h_{SC,1}$. Additionally, models $h_{\rm SC,2}$ and $h_{\rm SC,4}$ are related by a unitary transformation and a C_4 rotation around the z-axis so we will only consider $h_{SC,2}$ from now on. While we have focused on particular values of μ and Δ_0, the results do not change qualitatively as long as $\Delta_0 < \mu$, as is appropriate for the weak-pairing limit.

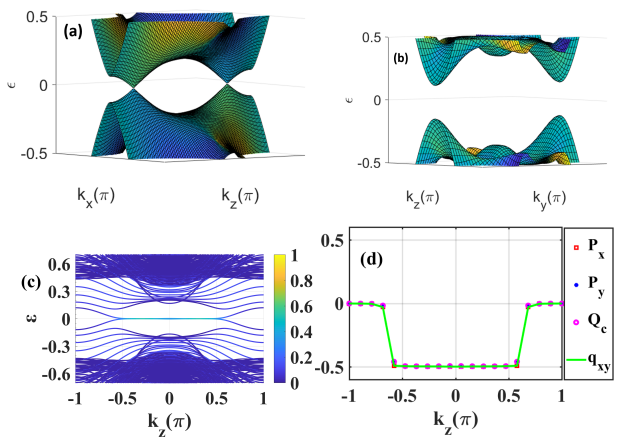

FIG. 2. The surface states of $h_{\mathrm{SC},1}$ in (a) $k_x - k_z$ and (b) $k_y - k_z$planes. (c) shows the Majorana hinges arc states in k_z direction; the color bar denotes the strength of the localization of the wave function at the corners. (d) depicts the P_x, P_y, Q_c and q_{xy} versus k_z. Color bars in (c) and the remaining hinge spectra in this article indicate localization of the states at hinge. The colors approaching 1 are the most localized.

We start by considering model $h_{\mathrm{SC},1}$. The pairing breaks C_4 symmetry, while retaining mirror symmetries, so the bulk nodes can be avoided and completely gapped[6] (see supplementary material (SM) [27] for more detail). However, we find that the surfaces $S_{y,\pm}$, perpendicular to the y-axis, exhibit two gapless nodes per surface, as Fig. 2 (a), whereas the ones perpendicular to the x-axis, $S_{x,\pm}$, are completely gapped, as Fig. 2 (b). We then obtain the bands for the hinges and find, as shown in Fig. 2 (c), that dispersionless hinge Majorana states are present at the four corners of the xy-plane for values of k_z between the two gapless nodes on the S_y surface. These states are reminiscent of the flat bands that appear between the nodes, and at the edges, of a 2D Dirac semimetal.

The structure of the spectrum and symmetry is similar to the one of path 2 quadrupolar semimetal in Ref. 25 and suggests that the presence of the boundary states, the hinge states in particular, might be due to a second-order topological invariant. To confirm it, we perform a superconducting analog of the nested Wilson loop calculation of the quadrupole moment $q_{xy}(k_z)$ for each k_z slice. To identify a quadrupole-like invariant for this superconducting system we separately evaluate the nested Berry phases $P_x(k_z), P_y(k_z)$ in the x and y directions [6] (in units of 2π), and the corner charge $Q_c(k_z)$, which takes values $0, 1/2$, to indicate the absence or presence of hinge states, all as a function of k_z. These are all effectively $\mathbb{Z}_2$ quantities, and a superconducting analog of the quadrupole invariant can be constructed using the relation $q_{xy}(k_z) \equiv (P_x(k_z) + P_y(k_z) - Q_c(k_z)) \mod 1$. Fig. 2 (d) shows that $P_x(k_z)$, $P_y(k_z)$ are quantized, and they take the non-trivial value for k_z in the interval between the two gapless nodes of the surfaces states on S_y, the same range of k_z for which we have hinge states. As a consequence we find that for values of k_z between the two surface nodes, $q_{xy}(k_z)$ is also non-trivial and therefore that the hinge states in model $h_{\mathrm{SC},1}$ are topologically protected in the presence of mirror symmetry and can be captured by a second-order, quadrupole-like, topological invariant. Interestingly, we find that the presence of the gapless nodes on the surface, and of the hinge states, is not affected by perturbations that break both mirror symmetries, and thus the hinge states are perturbatively stable when the BdG particle-hole symmetry is maintained even when the mirror symmetry is broken. The mirror symmetry is advantageous because it allows for a definitive calculation of the second-order invariant through nested Wilson loops, but it is not necessary. Due to the presence of Dirac nodes in the band structure of the surface states, and finite value of the quadrupole-like invariant we term superconductors like the one described by model $h_{\mathrm{SC},1}$ (and $h_{\mathrm{SC},13}$) *second order Dirac superconductors*. This is one of the main results of this work.

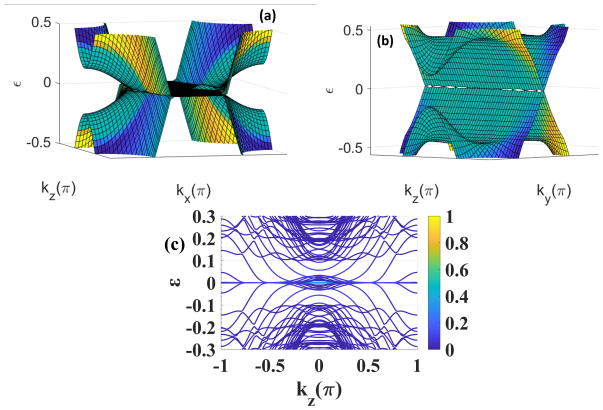

FIG. 3. The surface states of $h_{\mathrm{SC},2}$ in (a) $k_x - k_z$ and (b) $k_y - k_z$planes. (c) shows the Majorana hinges arc states in k_z direction.

Now consider model $h_{\mathrm{SC},2}$. The bulk states have nodal loops, (see SM [27]), and the surface states are gapless, as shown in Figs. 3 (a), (b). While we do find a small region of localized hinges states in the middle of the spectrum (see Fig. 3 (c)), the gapless bulk and surface states obscure them. It would be difficult to spectroscopically isolate the hinge modes of this model for any practical or experimental purpose. The same is true of model $h_{\mathrm{SC},4}$. Thus, while there may be some interesting features of the gapless bulk and surface states of these models left to explore, we leave the study of these model for future works given that in this work our primary interest is in hinge-mode phenomenology.

Models $h_{\mathrm{SC},5}$ and $h_{\mathrm{SC},6}$ differ from the previous models in that, in addition to the mirror symmetries $\mathcal{M}_x$ and $\mathcal{M}_y$, they retain C_4 symmetry in the superconducting state. As mentioned, model $h_{\mathrm{SC},5}$ has nodal points in the bulk quasiparticle spectrum, while $h_{\mathrm{SC},6}$ is fully gapped in the bulk (see SM [27]). We find that both models have gapless surface states but of different nature. Due to the C_4 symmetry, we only show the results for the surface states $S_{y,\pm}$. The surface bands of model $h_{\mathrm{SC},5}$ exhibit two nodal loops, see Fig. 4 (a),

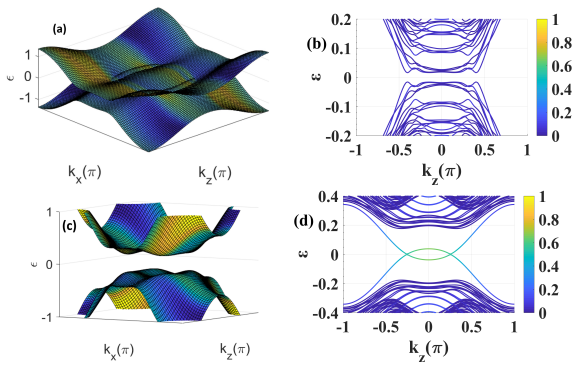

FIG. 4. Model $h_{\mathrm{SC},5}$: Surface states (a) in $k_x - k_z$ plane, and hinge states (b) along k_z, when $J_z = 0$, (c) and (d), same as (a) and (b), respectively, for the case when $J_z = 0.6$.

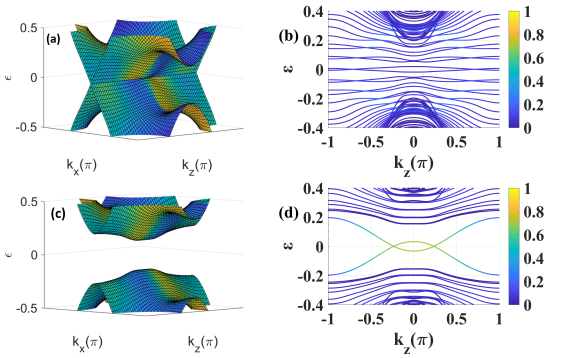

FIG. 5. Model $h_{\mathrm{SC},6}$: Surface states (a) in $k_x - k_z$ plane, and hinge states (b) along k_z, when $J_z = 0$, (c) and (d), same as (a) and (b), respectively, for the case when $J_z = 0.6$.

whereas the surface bands of model $h_{\mathrm{SC},6}$ exhibit a nodal line at $k_x = 0$ for the S_y surface states ($k_y = 0$ for the S_x surface states), Fig. 5 (a). Figure 4 (b) and Fig. 5 (b) show the bands for the hinges for models $h_{\mathrm{SC},5}$ and $h_{\mathrm{SC},6}$ and we see that there are no interesting localized hinge modes present.

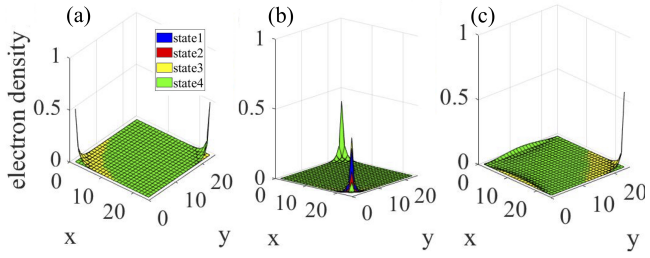

FIG. 6. Quasi-particle density of the corner states for model $h_{\mathrm{SC},6}$ in the presence of Zeeman term (a) $J_z = 0.4$ at $k_z = \pi/2$, (b) $J_z = -0.4$ at $k_z = \pi/2$ and (c) $J_z = 0.4$ plus $C_4\mathcal{M}_x$ breaking perturbation ($\tau_3 r_4 m_x$) with strength of 0.1 at $k_z = 0.2\pi$. Due to degeneracy, only some of the colors are visible and they overlap the other.

However, an external magneti field can perturb these systems to generate hinge modes. Let us apply a uniform magnetic field, or proximity-couple to a ferromagnet, to generate a Zeeman term $H_z = J_z\tau_3\sigma_3\kappa_0$, where J_z is directly proportional to the magnitude of the external magnetic field (we ignore any orbital effects of the magnetic field). This term qualitatively modifies the band structures of $h_{\mathrm{SC},5}$ and $h_{\mathrm{SC},6}$. From Figs. 4 (c), 5 (c) we see that the presence of the Zeeman term gaps out the the surface states completely (it also gaps out the bulk nodes of $h_{\mathrm{SC},5}$). Furthermore, we see the appearance of clear hinge states within the gap of the surface states, as shown in Fig. 4 (d) and Fig. 5 (d). H_z breaks C_4 symmetry and both mirror symmetries, but leaves the products $C_4\mathcal{M}_x$ (anti-diagonal mirror) and $C_4\mathcal{M}_y$ (diagonal mirror) intact. Because of these symmetries, and contrary to the hinge states of the other models discussed in this work, the hinge states of $h_{\mathrm{SC},5}$ and $h_{\mathrm{SC},6}$ (with Zeeman) are: dispersive, non-chiral, and localized only at two of the four hinges related by C_2 symmetry. In addition, we find that the pair of corners where the helical hinge states are localized switches upon a change of sign of the Zeeman term (e.g., switching the direction of the external magnetic field), see Fig. 6. This phenomenon could be useful for the experimental detection of these systems. For $J_z > 0$ ($J_z < 0$) there are two, counter-propagating modes at two of the four corners, and they are $\pm$ eigenstates of $C_4\mathcal{M}_y$ ($C_4\mathcal{M}_x$). The hinge modes are perturbatively stable even in the absence of the two $C_4\mathcal{M}_i$ symmetries as long as particle-hole symmetry is preserved. However, the modes can be destroyed through bulk or surface phase transitions. When strongly perturbting the system one can drive the system to various interesting configurations by breaking some of the symmetries. As an example, for $J_z > 0$ ($J_z < 0$) if we break $C_4\mathcal{M}_x$ ($C_4\mathcal{M}_y$), then the exchange symmetry between the two gapless hinges is broken. Strong perturbations can destroy the hinge states on one of the corners leaving a single pair of counter propagating modes on one of the corners left invariant under $C_4\mathcal{M}_y$ ($C_4\mathcal{M}_x$) (see Fig. 6 (c)).

In summary, in the presence of a Zeeman term, models $h_{\mathrm{SC},5}$ and $h_{\mathrm{SC},6}$ describe three-dimensional, magnetic field-induced second-order topological superconductors that are qualitatively different from the ones described by models $h_{\mathrm{SC},1}, h_{\mathrm{SC},3}$. They host hinge states only on two corners, and the pair of corners exhibiting the hinge states can be switched by a sign change of the Zeeman term. This is another main result of this work. We note that magnetic fields were also proposed to induce second-order topological superconductivity in a completely different system with different properties in two dimensions [28].

In conclusion, we have identified two types of second-order topological superconductors. The first type is a *second order Dirac superconductor* in which the presence of non-dispersive hinge states coexists with the gapless surface states. These superconductors can be described by a quadrupole-like, second order topological invariant. The second-type of higher-order superconductor is induced by a Zeeman term and manifests counter-propagating hinge modes on a single pair of corners. All of these superconducting states are generated in the weak-

pairing limit as s-wave superconducting pairing instabilities of a topological quadrupolar semimetal with a spin and an orbital degree of freedom. Possible interesting future research directions would be the study of the transport properties, and stability, of the surface and hinge states of the higher orders SC that we have identified in the presence of disorder and interactions It would be particularly interesting to compare these effects to the various anomalous transport properties, including phase-sensitive effects, that characterize the surface states of conventional topological superconductors [2, 29–36].

Acknowledgments.– S.A.A.G., X.H. and E.R. acknowledge support from ARO (Grant No. W911NF-18-1-0290), NSF (Grant No. DMR-1455233) and ONR (Grant No. ONR-N00014-16-1-3158). The numerical calculations have been performed on computing facilities at William & Mary which were provided by contributions from the NSF, the Commonwealth of Virginia Equipment Trust Fund, and ONR. TLH thanks the US National Science Foundation under grant DMR 1351895- CAR, and the MRSEC program under NSF Award Number DMR-1720633 (SuperSEED) for support.

[1] R. Resta, Reviews of Modern Physics **66**, 899 (1994).
[2] C.-K. Chiu, J. C. Y. Teo, A. P. Schnyder, and S. Ryu, Reviews of Modern Physics **88**, 035005 (2016).
[3] J. Zak, Phys. Rev. Lett. **62**, 2747 (1989).
[4] T. L. Hughes, E. Prodan, and B. A. Bernevig, Phys. Rev. B **83**, 245132 (2011).
[5] A. M. Turner, Y. Zhang, R. S. Mong, and A. Vishwanath, Phys. Rev. B **85**, 165120 (2012).
[6] W. A. Benalcazar, B. A. Bernevig, and T. L. Hughes, Science **357**, 61 (2017).
[7] W. A. Benalcazar, B. A. Bernevig, and T. L. Hughes, Physical Review B **96**, 245115 (2017).
[8] F. Schindler, A. M. Cook, M. G. Vergniory, Z. Wang, S. S. P. Parkin, B. A. Bernevig, and T. Neupert, Science Advances **4**, eaat0346 (2018).
[9] Z. Song, Z. Fang, and C. Fang, Phys. Rev. Lett. **119**, 246402 (2017).
[10] F. Schindler, Z. Wang, M. G. Vergniory, A. M. Cook, A. Murani, S. Sengupta, A. Y. Kasumov, R. Deblock, S. Jeon, I. Drozdov, H. Bouchiat, S. Guéron, A. Yazdani, B. A. Bernevig, and T. Neupert, Nature Physics **14**, 918 (2018).
[11] M. Ezawa, Phys. Rev. Lett. **120**, 026801 (2018).
[12] M. Ezawa, Phys. Rev. B **98**, 045125 (2018).
[13] J. Noh, W. A. Benalcazar, S. Huang, M. J. Collins, K. P. Chen, T. L. Hughes, and M. C. Rechtsman, Nature Photonics **12**, 408 (2018).
[14] C. W. Peterson, W. A. Benalcazar, T. L. Hughes, and G. Bahl, Nature **555**, 346 (2018).
[15] S. Imhof, C. Berger, F. Bayer, J. Brehm, L. W. Molenkamp, T. Kiessling, F. Schindler, C. H. Lee, M. Greiter, T. Neupert, and R. Thomale, Nature Physics **14**, 925 (2018).
[16] M. Ezawa, arXiv e-prints , arXiv:1807.10932 (2018), arXiv:1807.10932 [cond-mat.mes-hall].
[17] J. Langbehn, Y. Peng, L. Trifunovic, F. von Oppen, and P. W. Brouwer, Phys. Rev. Lett. **119**, 246401 (2017).
[18] Y. Wang, M. Lin, and T. L. Hughes, Phys. Rev. B **98**, 165144 (2018).
[19] E. Khalaf, Phys. Rev. B **97**, 205136 (2018).
[20] D. Călugăru, V. Juričić, and B. Roy, Phys. Rev. B **99**, 041301 (2019).
[21] Z. Wang, B. J. Wieder, J. Li, B. Yan, and B. A. Bernevig, arXiv e-prints , arXiv:1806.11116 (2018), arXiv:1806.11116 [cond-mat.mtrl-sci].
[22] B. J. Wieder and B. A. Bernevig, arXiv preprint arXiv:1810.02373 (2018).
[23] B. J. Wieder, Z. Wang, J. Cano, X. Dai, L. M. Schoop, B. Bradlyn, and B. A. Bernevig, Submitted (2018).
[24] W. A. Benalcazar, T. Li, and T. L. Hughes, arXiv preprint arXiv:1809.02142 (2018).
[25] M. Lin and T. L. Hughes, Phys. Rev. B **98**, 241103 (2018).
[26] T. Hashimoto, S. Kobayashi, Y. Tanaka, and M. Sato, Phys. Rev. B **94**, 014510 (2016).
[27] Supplementary material.
[28] X. Zhu, Phys. Rev. B **97**, 205134 (2018).
[29] L. Fu and C. L. Kane, Phys. Rev. Lett. **102**, 216403 (2009).
[30] L. Fu and C. L. Kane, Phys. Rev. B **79**, 161408 (2009).
[31] M. S. Foster and E. A. Yuzbashyan, Phys. Rev. Lett. **109**, 246801 (2012).
[32] M. S. Foster, H.-Y. Xie, and Y.-Z. Chou, Phys. Rev. B **89**, 155140 (2014).
[33] S. A. A. Ghorashi, S. Davis, and M. S. Foster, Phys. Rev. B **95**, 144503 (2017).
[34] S. A. A. Ghorashi, Y. Liao, and M. S. Foster, Phys. Rev. Lett. **121**, 016802 (2018).
[35] B. Roy, S. A. A. Ghorashi, M. S. Foster, and A. H. Nevidomskyy, arXiv:1708.07825v1.
[36] H.-Y. Xie, Y.-Z. Chou, and M. S. Foster, Phys. Rev. B **91**, 024203 (2015).